INTERFEROMETRIC SYNTHETIC APERTURE MICROSCOPY: PHYSICS-BASED IMAGE RECONSTRUCTION FROM OPTICAL COHERENCE TOMOGRAPHY DATA

Brynmor J. Davis, Tyler S. Ralston, Daniel L. Marks, Stephen A. Boppart and P. Scott Carney

Beckman Institute for Advanced Science and Technology,
Department of Electrical and Computer Engineering,
University of Illinois at Urbana-Champaign,
405 North Mathews Avenue, Urbana, Illinois 61801

ABSTRACT

Optical coherence tomography (OCT) is an optical ranging technique analogous to radar — detection of back-scattered light produces a signal that is temporally localized at times-of-flight corresponding to the location of scatterers in the object. However the interferometric collection technique used in OCT allows, in principle, the coherent collection of data, *i.e.* amplitude and phase information can be extracted. Interferometric Synthetic Aperture Microscopy (ISAM) adds phase-stable data collection to OCT instrumentation and employs physics-based processing analogous to that used in Synthetic Aperture Radar (SAR). That is, the complex nature of the coherent data is exploited to give gains in image quality. Specifically, diffraction-limited resolution is achieved throughout the sample, not just within focal volume of the illuminating field. Simulated and experimental verifications of this effect are presented. ISAM's computational focusing obviates the trade-off between lateral resolution and depth-of-focus seen in traditional OCT.

Index Terms— Optical Tomography, Optical Interferometry, Image Reconstruction, Inverse Problems, Microscopy

1. BACKGROUND

Optical coherence tomography [1, 2] uses light with a limited coherence length to probe a highly-scattering sample. The backscattered light is added to a reference field that is delayed by a time τ and focused on to a detector as shown in Fig. 1. Due to the short coherence length, the reference field only interferes with field back-scattered from a depth z in the sample where,

$$z = \frac{c\tau}{2}. \tag{1}$$

The optical path length to this depth is equal to the reference-arm optical path length. By scanning τ the object can be optically sectioned and a three-dimensional image constructed.

This work was supported in part by the National Institutes of Health (NIBIB, Roadmap Initiative, 1 R21 EB005321, to S.A.B.), the National Science Foundation (BES 05-19920, to S.A.B., CAREER Award, 0239265, to P.S.C.) and the Beckman Institute Graduate Fellowship Program (to T.S.R.).

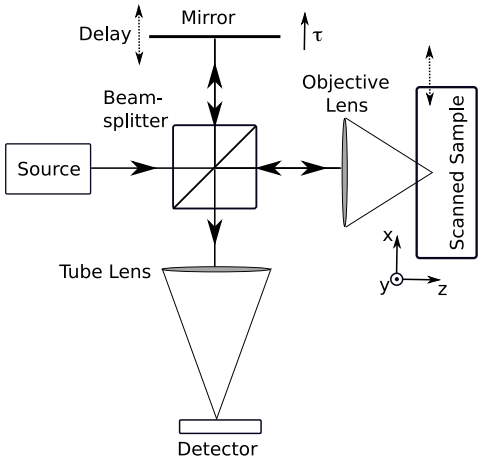

Fig. 1. Basic schematic of an optical coherence tomography system. Detection is performed using an interferometer with a delay (implemented here with a moveable mirror) inserted into the reference arm.

The axial (z) resolution of the system is determined by the coherence length of the probing light while the lateral (x-y) resolution is limited by the numerical aperture of the lens. Thus OCT data is typically modeled as,

$$s(x,y,\tau) = \int f(x',y',z') \times g(z' - z(\tau))h(x' - x, y' - y)\, dx'dy'dz', \tag{2}$$

where (x, y) is the lateral scan position, $z(\tau)$ is given by (1), f is the object to be imaged, g is determined by the coherence length of the light and h is the lateral beam-profile given by the objective lens. The coherence profile g is an autocorrelation function and can be calculated by taking the Fourier transform of the probing light's power spectrum.

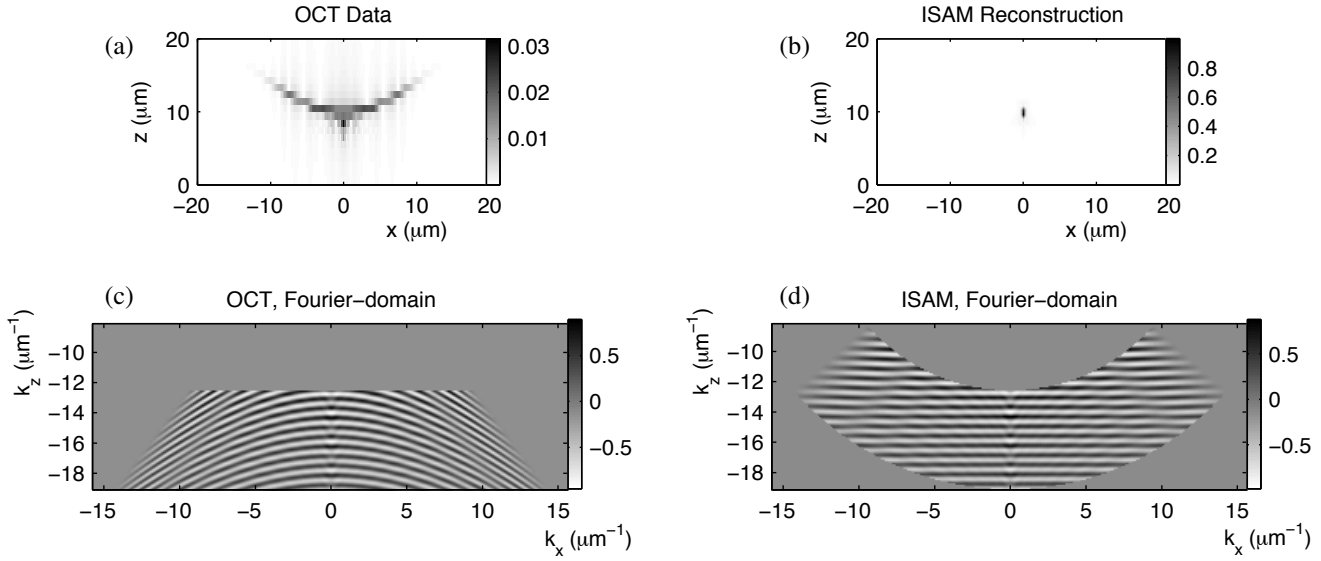

Fig. 2. Simulated OCT reconstruction from a point scatterer located at (0,0,10)μm (a) and the real part of its representation in the Fourier domain (c). ISAM's Fourier resampling takes the data shown in (c) to the reconstruction shown in (d). The corresponding spatial-domain representation (b) is more localized and of much higher magnitude. Note that Fourier transform of the object is a complex exponential oscillating in the k_z direction — this structure can be seen in (d) while the distortions associated with blurring can be seen in (c). The model uses a numerical aperture of 0.75 and the probing light spans wavelengths of 660nm to 1000nm.

2. INTERFEROMETRIC SYNTHETIC APERTURE MICROSCOPY

A recent series of papers [3, 4, 5, 6, 7, 8, 9] has demonstrated Interferometric Synthetic Aperture Microscopy. This method uses a model more comprehensive than shown in (2) to remove constraints on the depth-of-focus. The model given in (2) is valid only in the region in which the probing light is well collimated. Outside of this range the function $h(x, y)$ no longer accurately describes the beam profile and the data becomes blurred. This has led to the notion that the depth-of-focus and lateral resolution cannot be increased simultaneously — improving the lateral resolution requires a tighter focus which results in a beam that diverges after a shorter range in z. The ISAM methodology obviates this constraint by implementing a computational focusing of the data.

The apparatus shown in Fig. 1 uses a coherent (*i.e.* interferometric) detection system and can thus collect amplitude and phase data. This can be done by taking two phase shifted measurements to get in-phase and quadrature components [10] or by collecting the data in the Fourier domain using spectroscopic techniques [11] and applying the correct processing [12]. While traditional OCT systems do not fully exploit the complex nature of the data, ISAM collects a phase-stable complex data set by including a phase-reference structure (typically a cover-slip) in the object. An improved model is then used,

$$s(x, y, \tau) = \int f(x', y', z') \times g(z' - z(\tau))h(x' - x, y' - y, z')\, dx'dy'dz', \tag{3}$$

where the divergence of the focused light is modeled by including z-dependence in h.

Due to page constraints, the derivation of the ISAM reconstruction algorithm will not be given here, but can be found in [4]. ISAM processing consists of linear filtering and a remapping of coordinates in the Fourier domain. The data $s(x, y, \tau)$ goes to $S(k_x, k_y, \omega)$ in the Fourier domain while the estimate of the object has a Fourier transform defined on (k_x, k_y, k_z) coordinates. The ISAM mapping between ω and k_z is,

$$k_z(k_x, k_y, \omega) = \sqrt{\left(\frac{2\omega}{c}\right)^2 - k_x^2 - k_y^2}. \tag{4}$$

The ISAM algorithm consists of taking s to S, resampling according to (4), applying linear filters (Fourier-domain multiplication) and transforming back to spatial coordinates. An example of this process is shown in Fig. 2. The simulated data was generated using a fully vectorial electromagnetic model and without any small-angle approximations on the focused light [4, 13]. The ISAM reconstruction method used in Fig. 2 does not use any filtering after the resampling. The blurring in the OCT reconstruction and the focusing produced

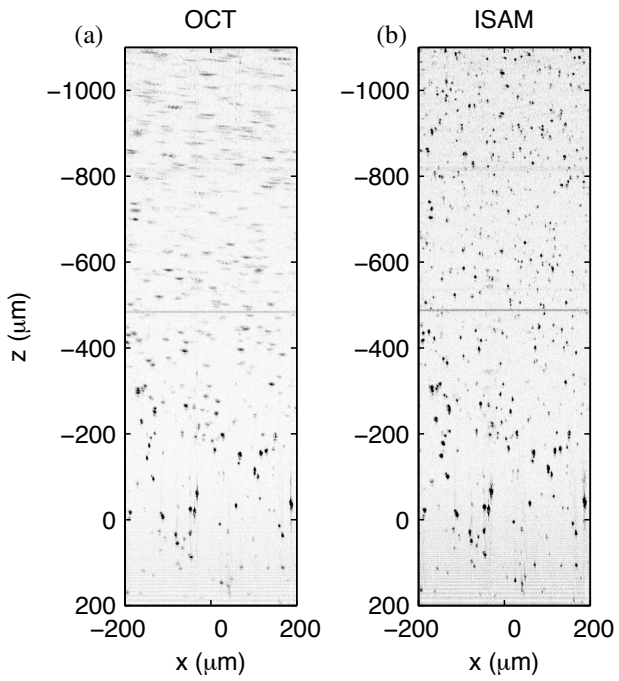

Fig. 3. OCT (a) and ISAM (b) reconstructions from real data. The focal plane in these images is at z=0. The reconstructions have been clipped to 10% of their maximum value so that low-level detail is visible.

by ISAM processing are clear. Traditional OCT reconstruction maps τ to z using (1) — this is equivalent to the map $k_z(k_x, k_y, \omega) = 2\omega/c$ in the Fourier domain (c.f. (4)). This simple scaling of axes, which is used to generate Fig. 2(c), does not produce any computational focusing.

The efficacy of ISAM processing has been demonstrated on biological samples [3]. It's effect on data from a manufactured phantom can be seen here in Fig. 3. The phantom consists of beads of titanium, with an average diameter of 1μm, suspended in silicone. An objective lens with a numerical aperture of 0.05 is used to collect light with a power-spectrum lying between wavelengths of 750nm and 850nm. It can be seen that the beads away from the focal plane are blurred in the OCT reconstruction but clearly imaged with ISAM.

3. ISAM AND SYNTHETIC APERTURE RADAR

OCT uses a time-of-flight signal to image axially in a manner analogous to radar systems. ISAM works with coherent data that is a function of a spatial offset and a time-of-flight — data of the same description is collected in SAR systems and also processed to synthesize an improved image [14]. Indeed, (4) can be recognized as the Stolt mapping which is commonly used in image reconstruction from strip-map SAR data [15]. This allows SAR processing techniques to be leveraged in understanding ISAM.

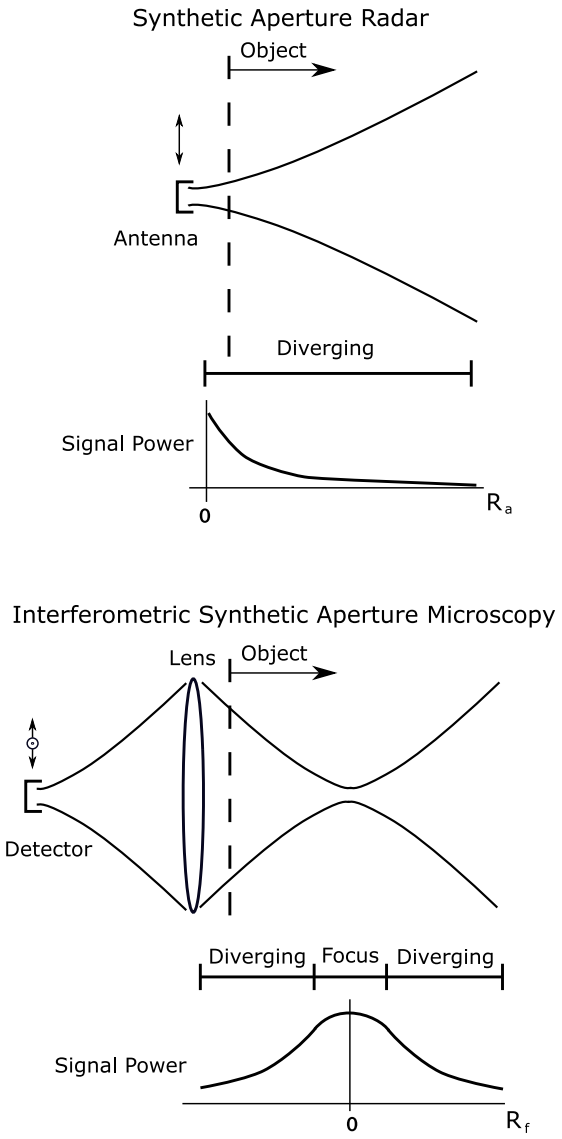

Fig. 4. Illustration of the differences in data collection between Synthetic Aperture Radar and Interferometric Synthetic Aperture Microscopy.

While the physics behind SAR and ISAM instruments result in the same Fourier-domain distortion, the systems are not entirely analogous. This is particularly evident when looking at the beam profiles illustrated in Fig. 4. Unlike SAR, ISAM operates in two distinct modalities within the object imaged. The focal region must be treated differently than the diverging areas of the beam. In certain non-standard cases, the Stolt mapping may not be appropriate for data originating from the focal region [4]. Additionally, SAR collects two-dimensional data while ISAM works in three dimensions. This affects the spreading losses of the system. ISAM exhibits a R_f^{-2} power decay where R_f is distance from the focal plane [4] while

SAR has a R_a^{-3} power dependence where R_a is the distance from the aperture. The lateral bandwidth of a SAR system is determined by the Fourier transform of the aperture, while the lateral bandwidth of an ISAM instrument is given by the ratio of the lens-aperture extent to the focal length.

4. DISCUSSION

Interferometric synthetic aperture microscopy gives computational focusing of OCT data in the same manner that SAR computationally focuses radar data. Since physical focusing is no longer needed to produce a sharp image, there is no depth-of-focus restriction to consider when choosing an objective lens in ISAM. In the past, high-resolution OCT systems using large numerical apertures have been described as Optical Coherence Microscopes (OCM) [16] and were understood to either image a single lateral plane or require the focus to be physically scanned in the z dimension. ISAM gives the high resolution associated with OCM but retains a large depth-of-focus. Rather than being limited by the range over which the probing light is collimated, the depth of focus is now limited by the noise level. The signal power (but not the resolution) drops with distance from the focal plane. The point at which it drops below the noise level determines the depth of focus in ISAM.

5. REFERENCES

[1] D. Huang, E. A. Swanson, C. P. Lin, J. S. Schuman, W. G. Stinson, W. Chang, M. R. Hee, T. Flotte, K. Gregory, C. A. Puliafito, and J. G. Fujimoto, "Optical coherence tomography," *Science*, vol. 254, pp. 1178–1181, 1991.

[2] J. M. Schmitt, "Optical coherence tomography (OCT): A review," *IEEE J. Select. Topics Quantum Electron.*, vol. 5, pp. 1205–1215, 1999.

[3] T. S. Ralston, D. L. Marks, P. S. Carney, and S. A. Boppart, "Interferometric synthetic aperture microscopy," *Nature Physics*, vol. 3, pp. 129–134, 2007.

[4] B. J. Davis, S. C. Schlachter, D. L. Marks, T. S. Ralston, S. A. Boppart, and P. S. Carney, "Nonparaxial vector-field modeling of optical coherence tomography and interferometric synthetic aperture microscopy," *J. Opt. Soc. Am. A*, (in press), 2007.

[5] T. S. Ralston, D. L. Marks, P. S. Carney, and S. A. Boppart, "Inverse scattering for optical coherence tomography," *J. Opt. Soc. Am. A*, vol. 23, pp. 1027–1037, 2006.

[6] T. S. Ralston, D. L. Marks, S. A. Boppart, and P. S. Carney, "Inverse scattering for high-resolution interferometric microscopy," *Opt. Lett.*, vol. 24, pp. 3585–3587, 2006.

[7] D. L. Marks, T. S. Ralston, S. A. Boppart, and P. S. Carney, "Inverse scattering for frequency-scanned full-field optical coherence tomography," *J. Opt. Soc. Am. A*, vol. 24, pp. 1034–1041, 2007.

[8] D. L. Marks, T. S. Ralston, P. S. Carney, and S. A. Boppart, "Inverse scattering for rotationally scanned optical coherence tomography," *J. Opt. Soc. Am. A*, vol. 23, pp. 2433–2439, 2006.

[9] B. J. Davis, T. S. Ralston, D. L. Marks, S. A. Boppart, and P. S. Carney, "Autocorrelation artifacts in optical coherence tomography and interferometric synthetic aperture microscopy," *Opt. Lett.*, vol. 32, pp. 1441–1443, 2007.

[10] P. Hariharan, *Optical Interferometry*, Academic Press, 2003.

[11] A. F. Fercher, C. K. Hitzenber, G. Kamp, and S. Y. El-Zaiat, "Measurement of intraocular distances by backscattering spectral interferometry," *Opt. Commun.*, vol. 117, pp. 43–48, 1996.

[12] Y. Zhao, Z. Chen, C. Saxer, S. Xiang, J. F. de Boer, and J. S. Nelson, "Phase-resolved optical coherence tomography and optical Doppler tomography for imaging blood flow in human skin with fast scanning speed and high velocity sensitivity," *Opt. Lett.*, vol. 25, pp. 114–116, 2000.

[13] B. Richards and E. Wolf, "Electromagnetic diffraction in optical systems. II. Structure of the image field in an aplanatic system," *Proc. R. Soc. London A*, vol. 253, pp. 358–379, 1959.

[14] J. C. Curlander and R. N. McDonough, *Synthetic Aperture Radar: Systems and Signal Processing*, Wiley-Interscience, 1991.

[15] P. T. Gough and D. W. Hawkins, "Unified framework for modern synthetic aperture imaging algorithms," *Int. J. Imag. Syst. Technol.*, vol. 8, pp. 343–358, 1997.

[16] J. A. Izatt, M. R. Hee, G. M. Owen, E. A. Swanson, and J. G. Fujimoto, "Optical coherence microscopy in scattering media," *Opt. Lett.*, vol. 19, pp. 590–592, 1994.